

Magnetism of layered chromium sulfides $M\text{CrS}_2$ ($M = \text{Li, Na, K, Ag, and Au}$): A first-principles study

A. V. Ushakov,^{1,2,3} D. A. Kukusta,^{2,4} A. N. Yaresko,^{2,*} and D. I. Khomskii¹¹*II Physikalisches Institut, Universität zu Köln, Zùlpicherstraße 77, D-50937 Köln, Germany*²*Max-Planck-Institut für Festkörperforschung, Heisenbergstraße 1, D-70569 Stuttgart, Germany*³*Institute for Theoretical Physics, Clausthal University of Technology, Leibnizstraße 10, D-38678 Clausthal Zellerfeld, Germany*⁴*Institute for Metal Physics, 36 Vernadskyi Bld., UA-03680 Kiev, Ukraine*

(Received 4 October 2012; published 14 January 2013)

$M\text{CrS}_2$ compounds ($M = \text{Li, Na, K, Cu, Ag, and Au}$) with triangular Cr layers show a large variety of magnetic ground states, ranging from 120° antiferromagnetic order of Cr spins in LiCrS_2 to double stripes in AgCrS_2 , helimagnetic order in NaCrS_2 , and, finally, ferromagnetic Cr layers in KCrS_2 . On the base of *ab initio* band structure calculations and an analysis of various contributions to exchange interactions between Cr spins, we explain this tendency as originating from a competition between antiferromagnetic direct nearest-neighbor d - d exchange and ferromagnetic superexchange via Sulfur p states, which leads to a change of sign of the nearest-neighbor interaction, depending on the radius of an M ion. It is shown that other important interactions are the third-neighbor interaction in a layer and interlayer exchange. We suggest that strong magnetoelastic coupling is probably responsible for the multiferroic properties of at least one material in this family, namely, AgCrS_2 .

DOI: [10.1103/PhysRevB.87.014418](https://doi.org/10.1103/PhysRevB.87.014418)

PACS number(s): 71.20.Lp, 71.70.Gm, 75.30.Et

I. INTRODUCTION

Frustrated magnetic systems are now attracting considerable attention.¹ Among them there are systems with very strong geometric frustrations (e.g., kagome and pyrochlore systems) and, also, less frustrated ones—e.g., systems with triangular lattices. Triangular magnets are overconstrained^{2,3} and most often they display one or the other type of magnetic ordering. Nevertheless, the frustrated nature of triangular layers strongly influences their magnetic properties, often making them rather unusual and very sensitive to small variations of the electronic and lattice structure.⁴ Such materials also present definite practical interest, e.g., as possible thermopower materials⁵ or new multiferroics.^{6,7}

The presence of orbital degeneracy may introduce special features in the properties of triangular magnets (see, e.g., Ref. 8). But even without such degeneracy, as in materials containing half-filled d (sub)shells ($\text{Fe}^{3+} d^5$, $\text{Cr}^{3+} t_{2g}^3$), the properties of such systems can be rather nontrivial.

Compared to similar materials with oxygen instead of sulfur, $M\text{CrS}_2$ compounds are much less studied. But it was recently shown that at least some of them, such as AgCrS_2 , show very interesting behavior: this particular material belongs to a pyroelectric class; below the Néel temperature $T_N = 50$ K, it develops a rather unusual double-stripe (DS) magnetic order⁹ and also becomes multiferroic.¹⁰ Motivated by these findings and trying to understand the reasons for this unusual type of magnetic ordering, apparently also relevant for the appearance of ferroelectricity, we undertook a study of this and similar systems with the M ions Li, Na, K, Cu, Ag, and Au. These systems—though, in principle, very similar and all containing as the main building block the same CrS_2 triangular layers—show very different magnetic orderings: from the pure nearest-neighbor antiferromagnetism (120° structure) for LiCrS_2 ,¹¹ with the smallest M cation, Li^+ , up to ferromagnetic (FM) CrS_2 layers in KCrS_2 ,¹² with the largest M ion, K^+ , with more complicated magnetic structures in the other systems. Our *ab initio* and model calculations allow us to explain the

general tendency of magnetic ordering in this very rich class of compounds, and this understanding may be helpful not only for these compounds, but also for other magnetic systems with triangular layers.

II. CRYSTAL AND MAGNETIC STRUCTURE

The crystal structure of the $M\text{CrS}_2$ series has been determined in Refs. 9 and 11–15. Cr atoms form a triangular lattice within CrS_2 layers, and the latter are joined by M atoms [Fig. 1(a)]. Cr atoms are located at the center of trigonally distorted octahedra composed of sulfur ions. Each S atom is shared by three different octahedra. But the “connection” between layers is different in different compounds. In compounds with alkali metals, Li, Na, and K are also sitting in S_6 octahedra. One can visualize the structure of these compounds as originating from the rock-salt structure of (actually hexagonal) CrS , in which Cr and alkali ions are ordered in consecutive (1,1,1) planes, so that Cr as well as Li, Na, or K is octahedrally coordinated by anions (the detailed stacking of Cr, S, and alkali layers may be different).

At the same time, the structure of the systems $M\text{CrS}_2$ with $M = \text{Cu, Ag, and Au}$ is different. In corresponding oxides the nonmagnetic ions Cu^{1+} and Au^{1+} with configuration d^{10} are linearly coordinated. They are located in the centers of oxygen dumbbells, i.e., are sandwiched between two oxygens belonging to different MO_2 layers. The resulting structure is that of delafossites.¹⁶

The structure of their sulfur analogs is more interesting: it is “in between” that of, say, LiCrO_2 ¹⁷ and AgCrO_2 . These M^+ ions are located above the center of an S_3 triangle in one—say, the lower CrS_2 —layer but are connected by vertical bonds to one S^{2-} ion in the next, upper layer [Fig. 1(c)]. In effect Cu, Ag, and Au are in a “tripod” made of four S ions, or in a distorted (elongated in the c direction) S_4 tetrahedron. Metal ions in such S_4 tetrahedra are strongly shifted towards the upper, apical S ion. All such tripods, or tetrahedra, are pointing in the same

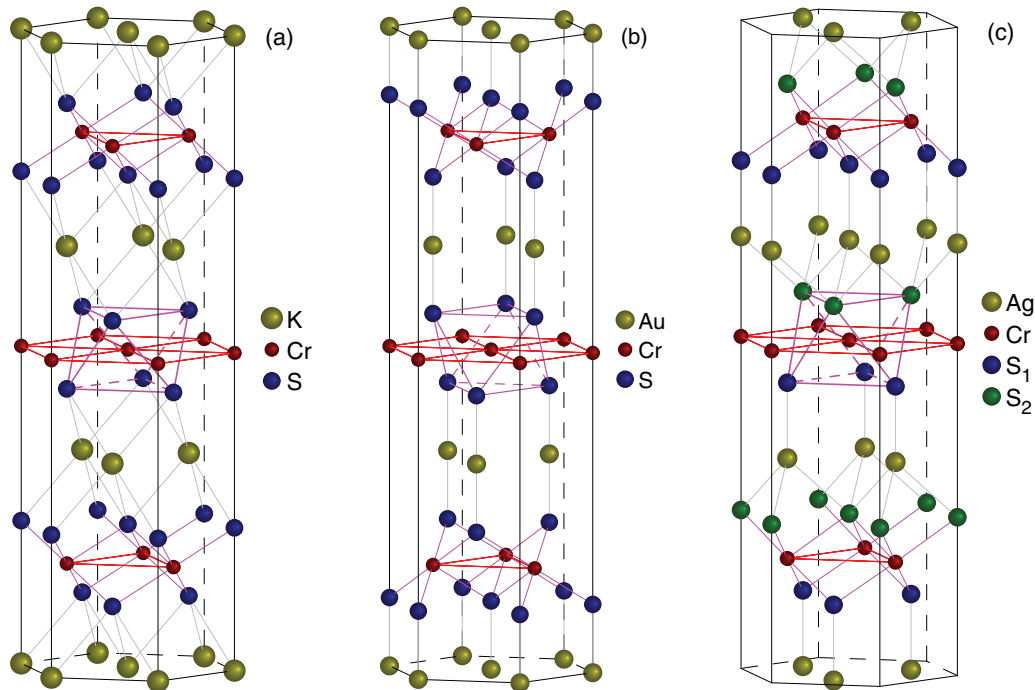


FIG. 1. (Color online) High-temperature rhombohedral crystal structures of KCrS_2 (a), AuCrS_2 (b), and AgCrS_2 (c). Also shown is a distorted CrS_6 octahedron surrounding a Cr ion in the cell center.

direction, e.g., up, so that the resulting structure does not have an inversion symmetry and is of a pyroelectric class. However, this interesting structural feature, though probably important for some properties of these materials, seems to play a minor role in the magnetic properties of these compounds, which mainly depend on interactions in CrS_2 layers. Whereas most structural studies of $M\text{CrS}_2$ with $M = \text{Cu}$ and Ag give the structure with M ions in sulfur “tripods” and $R\bar{3}m$ symmetry,⁸ there are also reports of a different crystal structure. Thus, in a recent paper¹⁵ it is concluded that the symmetry of AuCrS_2 is $R\bar{3}m$ and the actual structure is the delafossite one with linearly coordinated Au^+ [Fig. 1(b)].

$M\text{CrS}_2$ compounds have diverse magnetic structures and a broad set of physical properties. Being coupled antiferromagnetically between the layers, they exhibit quite different in-plane ordering at low temperatures.

At high temperatures (HTs) LiCrS_2 belongs to the $P\bar{3}m1$ space symmetry group. According to neutron scattering measurements the magnetic structure of this compound below the Néel temperature $T_N = 55$ K exhibits a triangular spin arrangement (120° structure) within the triangular planes, with adjacent planes being coupled antiferromagnetically.^{11,18} This structure is typical for Heisenberg antiferromagnets with nearest-neighbor coupling on a triangular lattice. The observed value of the Cr^{3+} spin magnetic moment equals $2.26\mu_B$, which is considerably smaller than the expected value of $3\mu_B$. The difference presumably may be attributed to covalency effects, which can considerably alter the distribution of the spin density around the Cr^{3+} ion. Indeed, one can expect such behavior, keeping in mind the much smaller size of Li^+ ions and respective reduction in unit cell volume.

KCrS_2 undergoes an antiferromagnetic (AFM) transition at $T_N = 38$ K.¹² The symmetry group at HT is rhombohedral

$R\bar{3}m$. The magnetic structure, in contrast to LiCrS_2 , consists of FM layers perpendicular to the c axis, which are antiferromagnetically coupled to adjacent ones. The paramagnetic Curie temperature of KCrS_2 is not low ($\theta_C = 112$ K) and indicates that the FM interaction in the planes is the dominant one. The observed value of the Cr^{3+} spin magnetic moment ($3.04 \pm 0.05\mu_B$) obtained by neutron scattering¹² is in good agreement with the expected value of $3\mu_B$ and with the value obtained from the susceptibility measurements ($3.1\mu_B$). This can be interpreted as an indication that in KCrS_2 covalency effects are relatively weak.

In contrast to LiCrS_2 and KCrS_2 , AgCrS_2 undergoes, at $T_N = 41.6$ K, a first-order phase transition from a paramagnetic rhombohedral $R\bar{3}m$ structure to an AFM monoclinic Cm structure.⁹ Most interesting, the material was found to be ferroelectric below T_N ; i.e., it is a multiferroic system.¹⁰ Note that this phenomenon differs from the eventual polarization of AgCrS_2 due to its pyroelectric crystal structure: this polarization appears only in a magnetically ordered state and lies in the ab plane, not along the c direction, as the eventual pyroelectric polarization due to the crystal structure itself. In addition to being ferroelectric below T_N , the low-temperature phase of AgCrS_2 exhibits an unconventional collinear magnetic structure that can be described as double FM stripes coupled antiferromagnetically, with the magnetic moment of Cr^{3+} aligned along the b axis within the anisotropic triangular plane. Ferroelectricity below T_N in AgCrS_2 is explained as a consequence of atomic displacements at the magnetoelastically induced structural distortion, most probably driven by the DS magnetic structure itself. Thus, this system can be classified as a type II multiferroic.^{6,7,19}

Similarly to AgCrS_2 , AuCrS_2 undergoes a first-order magnetic and structural phase transition at $T_N = 47$ K from

TABLE I. Cr-Cr ($d_{\text{Cr-Cr}}$) and Cr-S ($d_{\text{Cr-S}}$) interatomic distances (in Å) as well as Cr-S-Cr bond angles θ (in deg) for the high-temperature $M\text{CrS}_2$ structures. For $M = \text{Cu}$ and Ag only the averaged $d_{\text{Cr-S}}$ is shown, while θ is given for two inequivalent S ions.

M	$d_{\text{Cr-Cr}}$	$d_{\text{Cr-S}}$	θ	Magnetic structure
Li	3.4515	2.4063	91.7	AFM 120°
Cu	3.4728	2.4036	90.6, 94.6	Spiral ordering
Au	3.4826	2.3862	93.7	AFM double stripes
Ag	3.4979	2.4085	92.2, 94.1	AFM double stripes
Na	3.5561	2.4249	94.3	Spiral ordering
K	3.6010	2.4123	96.6	FM in-plane

a paramagnetic rhombohedral $R\bar{3}m$ to a monoclinic AFM $C2/m$ structure.¹⁵ The simultaneous observation of magnetic and structural transition in both AgCrS_2 and AuCrS_2 gives evidence of a large magnetoelastic coupling in these systems. This coupling accounts for the stability of the observed magnetic order, considering that the structural distortions at the transition suppress the geometric frustration of the Cr layers. As we show below, the peculiar AFM structure observed in both AgCrS_2 and AuCrS_2 is explained by the interplay of the exchange due to direct dd hopping and that via anions (sulfur) involving nearest-neighbor and farther-neighbor Cr-Cr interactions, as well as the residual frustration in the triangular Cr planes.

In Table I we list different compounds in order of increasing Cr-Cr distance, which also corresponds to an increase in a Cr-S-Cr bond angle since average Cr-S distances vary much less than Cr-Cr ones. One immediately notices a definite correlation between the crystal structure and the magnetic order: with increasing Cr-Cr distance and Cr-S-Cr angle, the magnetic structure changes from a 120° AFM structure in LiCrS_2 , with the smallest, Li^+ ion and the shortest Cr-Cr distance, to FM layers in KCrS_2 , with the largest, K^+ ion and the longest Cr-Cr distance. The crossover between these limiting cases occurs via incommensurate magnetic phases in CuCrS_2 and NaCrS_2 and the DS structure in AuCrS_2 and AgCrS_2 . It is this correlation between crystal and magnetic structure that is the main topic of our study. We approach this problem by performing *ab initio* calculations, in which we obtain the electronic structure of the $M\text{CrS}_2$ compounds, as well as the values of relevant exchange constants. We then analyze the observed general trends in a superexchange model, discussing different relevant, often competing contributions to the total exchange.

III. COMPUTATION DETAILS

Band structure calculations were performed using the linear muffin-tin orbitals (LMTO) method²⁰ as implemented in the PY-LMTO computer code.²¹ We used the Perdew-Wang²² parametrization for the exchange-correlation potential in the local spin-density approximation (LSDA). Brillouin-zone integrations were performed using the improved tetrahedron method.²³

When spin-orbit coupling is not taken into account, the use of the generalized Bloch theorem²⁴ makes possible self-consistent calculations of the band structure and the total energy $E(\mathbf{q})$ for spin-spiral structures with an arbitrary wave

vector \mathbf{q} as described in detail in Refs. 25 and 26. In these calculations the magnetization direction in an atomic sphere centered at $\mathbf{t} + \mathbf{R}$, where \mathbf{t} specifies its position in a unit cell and \mathbf{R} is a translation vector, is defined by two polar angles θ and $\phi = \mathbf{q} \cdot \mathbf{R} + \phi_0$. In the present work we considered only planar spin spirals with all $\theta = \pi/2$. The phase ϕ_{Cr} inside spheres surrounding Cr ions was fixed by requiring $\phi_{\text{Cr}} = \mathbf{q} \cdot \mathbf{t}_{\text{Cr}}$, whereas for all other spheres it was determined self-consistently by diagonalizing the corresponding spin-density matrix.

This general approach allows us not only to treat on the same footing collinear, e.g., FM or stripe, and noncollinear, e.g., 120° AFM, *commensurate* magnetic structures, but also to perform calculations for *incommensurate* helical structures. The only restriction is that it should be possible to describe the magnetic structure by a single wave vector \mathbf{q} . After the \mathbf{q} dependence of the total energy has been calculated, effective exchange interactions between Cr spins can be obtained by mapping $E(\mathbf{q})$ onto a relevant Heisenberg-like model.

The magnetocrystalline anisotropy was estimated by using the force theorem,²⁷ i.e., by comparing band energies obtained for selected collinear spin structures from spin-polarized relativistic calculations with the magnetization parallel to different crystallographic axes. Spin-orbit coupling in these calculations was included in the LMTO Hamiltonian at the variational step.²⁸

In order to study the effect of relatively strong electronic correlations in the Cr d shell on the band structure and magnetic interaction in $M\text{CrS}_2$ compounds, for some of them we also calculated $E(\mathbf{q})$ using the rotationally invariant LSDA + U method.²⁹ For the double counting term the so-called atomic limit was used.³⁰ Other details on the implementation of the LSDA + U method in the PY-LMTO code are given in Ref. 31. Calculations were performed for the Hund's exchange coupling parameter $J = 0.9$ eV and the on-site Coulomb repulsion $U = 1.9, 2.9,$ and 3.9 eV, which gives 1, 2, and 3 eV for $U_{\text{eff}} = U - J$.

IV. RESULTS AND DISCUSSION

A. Band structure and energies of different magnetic structures

Our band-structure calculations demonstrate that all atoms in $M\text{CrS}_2$ compounds exhibit their valences corresponding to the stoichiometry of the compound, i.e., the atomic charges correspond to M^+ , Cr^{3+} , and S^{2-} . The s orbitals of M^+ are empty, whereas the p orbitals of S^{2-} are fully occupied. Since the Cr atom is triply ionized, there are three d electrons localized on a Cr^{3+} ion.

The octahedral crystal field at the Cr site causes the d orbitals to split into a triplet t_{2g} (xy, xz, yz) and a doublet e_g ($3z^2 - r^2, x^2 - y^2$), with the energy of the t_{2g} orbitals being lower than that of the e_g states. Since there are three d electrons localized on a Cr site, in spin-restricted band structure calculations the t_{2g} states are half-filled, whereas the e_g levels are empty. In spin-polarized calculations the spin-up t_{2g} states are occupied, and spin-down t_{2g} are empty.

The cubic component of the crystal field at the Cr site is strong enough for the t_{2g} and e_g orbitals to form two nonoverlapping sub-bands separated by an energy gap of about

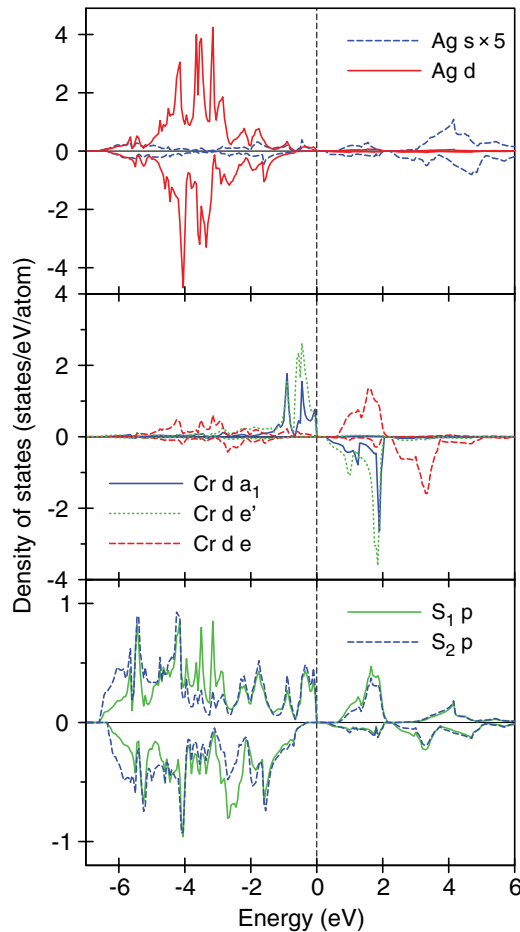


FIG. 2. (Color online) Partial densities of states in AgCrS_2 with the FM alignment of Cr moments. Energies are given relative to the Fermi level E_F .

0.5 eV. Additional trigonal distortion along the c axis lifts the degeneracy of the t_{2g} levels and splits them into a singlet a_{1g} and a doublet e'_g (a_1 and e' in compounds with $R3m$ symmetry, e.g., AgCrS_2), which are linear combinations of the t_{2g} orbitals. Three Cr^{3+} d electrons occupy spin-up a_{1g} and e'_g orbitals.

The electronic structures and density of states (DOS) of compounds in $M\text{CrS}_2$ series are similar, so to get details specific for current calculations, we consider as an example the DOS curves obtained for AgCrS_2 in FM spin-polarized LSDA calculations (see Fig. 2). The occupied part of the valence band can be subdivided into several regions. For all M ions their valence s states are empty and d states (if they exist) are totally occupied. These valence s and d states do not contribute to the electronic density close to the Fermi energy E_F . In AgCrS_2 the Ag $4d$ states appear between -6 and -1.5 eV.

The occupied S^{2-} $3p$ states form a broad band with the width of 6 eV between -6.5 and -0.3 eV, being strongly hybridized with both Ag $4d$ and Cr $3d$ states. As discussed later, this hybridization between Cr $3d$ and S $3p$ states is responsible for superexchange along the Cr-S-Cr and Cr-S-S-Cr paths. According to our band structure calculations these materials are insulating even in the FM state and even without including Hubbard's U . For instance, for AgCrS_2 the LSDA gives an energy gap of 0.55 eV. That is, due to their specific electronic

structure—half-filled t_{2g} subshell and empty e_g states of Cr^{3+} —they would be band insulators (in a magnetically ordered state). When electronic correlations are accounted for in LSDA + U calculations, the occupied majority-spin t_{2g} states are shifted by $U_{\text{eff}}/2$ to lower energies, whereas the unoccupied minority-spin t_{2g} and all e_g states move $\sim U_{\text{eff}}/2$ to higher energies, which increases the values of the gaps.

Magnetic properties and the electronic structure of $M\text{CrS}_2$ compounds are closely related to the occupancy of the Cr $3d$ states, which are spread over a wide energy interval, from -6 to 4 eV, and form two nonoverlapping sub-bands separated by an energy gap. Cr e_g and t_{2g} orbitals form $pd\sigma$ and $pd\pi$ bonds with sulfur p orbitals, respectively. The hybridization between occupied Cr spin-up t_{2g} and S p states at -1 and -0.5 eV is clearly observed. Being rather small below E_F , the hybridization between Cr d and S p above E_F is larger for e_g states and is well pronounced for spin-up DOS values.

Our calculations prove the clearly insulating nature of these materials. The exchange splitting $\Delta_{\text{ex}} \sim 2$ eV is prominent for Cr $3d$ bands in the whole $M\text{CrS}_2$ series where only spin-up Cr a_{1g} and e'_g orbitals are filled.

The calculated values of the Cr spin magnetic moment are close to $3\mu_B$ for all compounds in the series. Calculations for spin spirals showed that the Cr moment depends only weakly on the wave vector of a spiral, i.e., on the kind of magnetic order. In LiCrS_2 , for instance, the moment varies from $2.74\mu_B$ for the 120° AFM structure to $2.98\mu_B$ for the FM one. This also confirms the localized character of the Cr moments and suggests that magnetic interactions between them can be described by the Heisenberg model.

Damay *et al.*, in Ref. 9, analyzed dynamic correlations and found a small spin gap at very low energies as $\mathbf{q} \rightarrow 0$ that has been attributed to the weak magnetic anisotropy; i.e., we conclude that the Cr spins in $M\text{CrS}_2$ are relatively isotropic and can be described by the Heisenberg model. The localized character of Cr^{3+} spin magnetic moments is confirmed in our calculations by the fact that Cr spin-up a_{1g} and e'_g states are fully occupied, localized on the Cr^{3+} site, and separated from empty states by an energy gap.

The applicability of the Heisenberg model allows us to investigate the wide range of Cr spin moment configurations within the single approach using the Heisenberg Hamiltonian in the form

$$H = \frac{1}{2} \sum_{i \neq j} J_{ij} \mathbf{S}_i \mathbf{S}_j. \quad (1)$$

Everywhere below we work in the orthogonal coordinates, choosing the y axis along one of the directions between Cr-Cr nearest neighbors in the ab plane, and the x axis is chosen perpendicular to it; i.e., it points from one Cr to its second neighbor (see Fig. 3). Thus, in our notation the \mathbf{q} vectors of magnetic superstructures are given in these coordinates, not in the standard vectors of corresponding reciprocal lattices. We measure the in-plane components of a \mathbf{q} vector in units of $2\pi/a$ and the out-of-plane component in units of $2\pi/c$.

In the case of an arbitrary wave vector $\mathbf{q} = (q_x, q_y, q_z)$ the Heisenberg magnetic energy in these coordinates is

$$E(\mathbf{q}) = \epsilon_1(\mathbf{q}) + \epsilon_2(\mathbf{q}) + \epsilon_3(\mathbf{q}) + \epsilon_z(\mathbf{q}), \quad (2)$$

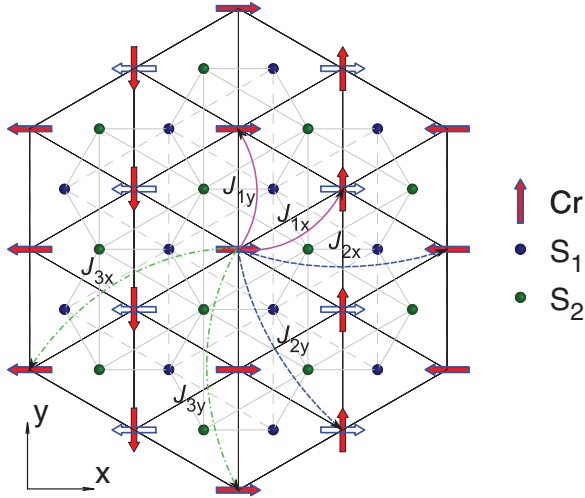


FIG. 3. (Color online) Representation of double-stripe [open (blue) arrows] and 90° [filled (red) arrows] magnetic structures within the Cr plane. One underlying (S_1) and one overlying (S_2) sulfur layer are shown as well. Low-temperature intraplane exchanges between the first (J_{1x} , J_{1y}), the second (J_{2x} , J_{2y}), and the third (J_{3x} , J_{3y}) neighbors are shown as curved lines with arrows. In the high-temperature phase $J_{1x} = J_{1y} = J_1$, $J_{2x} = J_{2y} = J_2$, and $J_{3x} = J_{3y} = J_3$.

where $\epsilon_i(\mathbf{q})$ are contributions proportional to the exchange coupling constants J_i between i th Cr neighbors within the triangular plane (see Fig. 3). For undistorted HT rhombohedral structures,

$$\epsilon_1(\mathbf{q}) = J_1[2 \cos(\sqrt{3}q_x a/2) \cos(q_y a/2) + \cos(q_y a)], \quad (3)$$

$$\epsilon_2(\mathbf{q}) = J_2[\cos(q_x a \sqrt{3}) + 2 \cos(\sqrt{3}q_x a/2) \cos(3q_y a/2)], \quad (4)$$

$$\epsilon_3(\mathbf{q}) = J_3[2 \cos(q_x a \sqrt{3}) \cos(q_y a) + \cos(2q_y a)]. \quad (5)$$

An expression for interlayer coupling, $\epsilon_z(\mathbf{q})$, is particularly simple for LiCrS_2 :

$$\epsilon_z(\mathbf{q}) = J_z \cos(q_z c). \quad (6)$$

In other compounds with abc stacking of Cr layers Cr neighbors in adjacent planes sit above and below the centers of triangles, i.e., above S_1 and below S_2 positions in Fig. 3, and $\epsilon_z(\mathbf{q})$ becomes

$$\begin{aligned} \epsilon_z(\mathbf{q}) = J_z[2 \cos(q_z c/3 - q_x a/(2\sqrt{3})) \cos(q_y a/2) \\ + \cos(q_z c/3 + q_x a/\sqrt{3})]. \end{aligned} \quad (7)$$

When J_z is sufficiently strong it may affect the in-plane magnetic order.

As sketched in Fig. 3, in the monoclinic low-temperature (LT) phases of AgCrS_2 and AuCrS_2 exchange interactions, J_{nx} and J_{ny} , between n th neighbors along the x and y directions are no longer equal and expressions (3)–(5) should be modified accordingly. For instance, the energy of the nearest-neighbor interaction becomes

$$\epsilon_1(\mathbf{q}) = 2J_{1x} \cos(q_x x_{1x}) \cos(q_y y_{1x}) + J_{1y} \cos(q_y y_{1y}), \quad (8)$$

where a vector $\mathbf{r}_{1x/y}$ ($x_{1x/y}, y_{1x/y}, 0$) connects a Cr site with its nearest neighbors along the x and y directions.

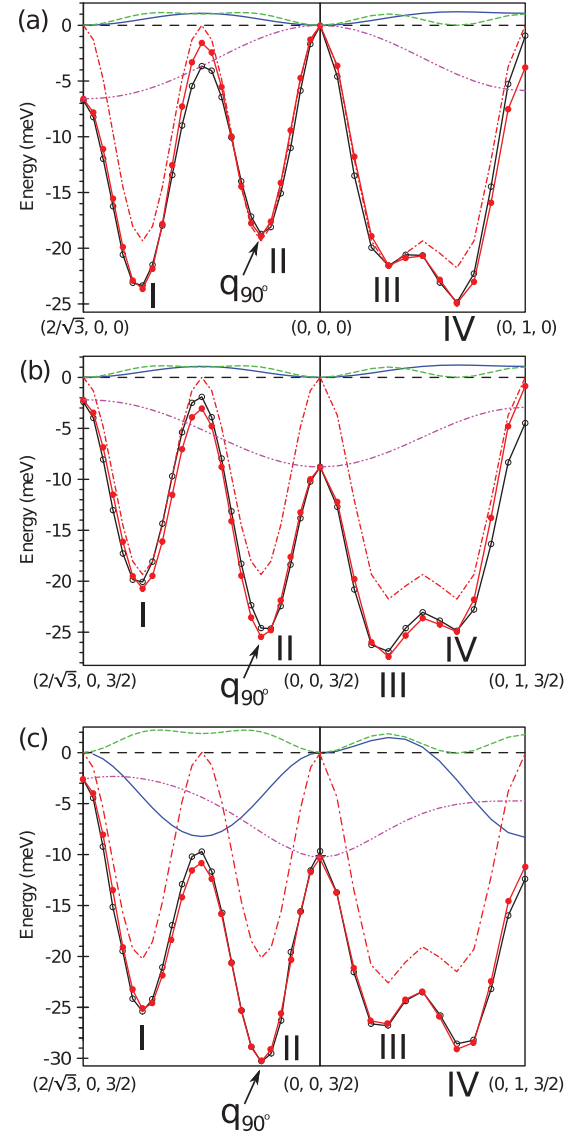


FIG. 4. (Color online) Calculated [open (black) circles] and fitted [filled (red) circles], using the least-squares method in the Heisenberg model, profiles $E(\mathbf{q})$ of magnetic energies for AgCrS_2 for two sets of wave vectors; see the text. Partial contributions in magnetic energy, calculated according to Eqs. (3)–(7), are shown as well. The $\epsilon_1(\mathbf{q})$, $\epsilon_2(\mathbf{q})$, $\epsilon_3(\mathbf{q})$, and $\epsilon_z(\mathbf{q})$ profiles are represented by solid (blue), dashed (green), dashed with one dot (red), and dashed with two dots (magenta) lines. The dispersion curves shown in (a) and (b) are calculated for the high-temperature phase with ferro (a) and antiferro (b) interlayer ordering, whereas those in (c) are calculated for the low-temperature structure and antiferro interlayer ordering. The 90° structure, by which we model the double-stripe magnetic structure observed in AgCrS_2 and AuCrS_2 , is marked by the arrow.

In order to estimate the effective exchange parameters J_i and J_z we first carried out *ab initio* calculations for a number of \mathbf{q} vectors lying in the $q_z = 0$ [Fig. 4(a)] and $q_z = 3/2$ [Fig. 4(b)] planes. The latter value of q_z results in a 180° rotation of Cr spins in adjacent layers. We then fitted the \mathbf{q} dependence of the calculated total energy $E(\mathbf{q})$ [open (black) circles in Fig. 4] by the Heisenberg model given by Eqs. (2)–(7) using a least-squares fit with four (J_1 , J_2 , J_3 , and J_z) and seven

($J_{1x,1y}$, $J_{2x,2y}$, $J_{3x,3y}$, and J_z) exchange parameters for the HT and LT phases, respectively. The results of such a fit for the most interesting system, AgCrS_2 , which has the unusual DS magnetic structure and becomes multiferroic below T_N , are shown in Fig. 4 by filled (red) circles. The good agreement between the result of the LSDA total energy calculation and that of the fit proves the possibility of describing the magnetic properties of these compounds by the Heisenberg model, which includes the exchange coupling constants between first, second, and third neighbors, plus the interlayer exchange constant J_z . From these calculations we can extract the values of the exchange constants for different materials, and by comparing the energies of different states we can determine which state will be the ground state for one or the other system.

B. Magnetic structures

Let us discuss the nature of different competing states, i.e., different minima of $E(\mathbf{q})$ in Fig. 4. The 120° AFM spin structure observed in LiCrS_2 , in Ref. 11, is realized by a spin spiral with $\mathbf{q} = (0, 2/3)$ (in units of $2\pi/a$), which gives the minimum IV in Fig. 4. The local minimum III corresponds to 120° AFM order in the sublattice of third Cr neighbors.

The FM in-plane structure observed in KCrS_2 in Ref. 12 corresponds to $\mathbf{q} = 0$. In contrast, the magnetic energy of AgCrS_2 (Fig. 4) has a maximum instead of a minimum at this \mathbf{q} , which agrees with the fact that for this system the dominant exchange interactions are AFM.

The DS spin structure observed in AgCrS_2 cannot be represented as a single \mathbf{q} spiral if the rhombohedral unit cell of the HT $R3m$ structure is used. However, it can be easily verified that with our choice of axes the Heisenberg energy of the DS structure is exactly equal to the energy of a spin spiral with $\mathbf{q}_{90^\circ} = (\sqrt{3}/6, 0)$, shown by filled (red) arrows in Fig. 3, in which spins of each i th Cr chain running along the y direction turn by 90° with respect to the previous ($i - 1$) one.

Indeed, let us consider the interaction of a Cr spin from some ($i = 0$) chain with the rest of the Cr plane. In the DS structure the spin directions in odd chains to the left ($-2|i| + 1$) and to the right ($2|i| + 1$) are opposite and their contributions to the magnetic energy $J\mathbf{S}_0 \cdot \mathbf{S}_{2|i|+1} = -J\mathbf{S}_0 \cdot \mathbf{S}_{-2|i|+1}$ cancel each other. In the 90° structure odd chains do not contribute to the magnetic energy because of the orthogonality of Cr spins in odd and even chains ($J\mathbf{S}_0 \cdot \mathbf{S}_{2i+1} = 0$). Consequently, the magnetic energy is determined by the interaction of \mathbf{S}_0 with \mathbf{S}_{2i} from the even chains, which are exactly the same in both spin structures. Here we assume that the exchange coupling constants of \mathbf{S}_0 with spins from chains to the left $\mathbf{S}_{-|i|}$ and to the right $\mathbf{S}_{|i|}$ are equal. The couplings between n th neighbors lying in the same (J_{ny}) and different (J_{nx}) chains need not be equal so that the degeneracy of the DS and 90° structures also holds for distorted Cr layers of the monoclinic LT phase of AgCrS_2 .

LSDA supercell calculations performed for the DS and 90° structures also gave the total energies, which are equal within the numerical accuracy, with their energy difference being less than 1 meV per Cr ion. Because of the degeneracy of the two spin structures the energy of the DS structure can be calculated within the same spin-spiral approach as the energies of other competing magnetic states. The corresponding energy minimum is labeled “II” in Fig. 4.

Experimentally, however, these two structures would lead to somewhat different features of neutron scattering spectra, although the positions of magnetic Bragg peaks are the same. The authors of Ref. 9 concluded that the DS structure fits the experimental data better than the 90° structure.

The same 90° structure within a Cr plane is also realized at $\mathbf{q} = (3\sqrt{3}/6, 0)$, corresponding to minimum I in Fig. 4. However, because of the rather strong interlayer coupling given by Eq. (7), the energies at minima I and II are not equal. Finally, the maximum at $\mathbf{q} = (2\sqrt{3}/6, 0)$ between these two minima corresponds to single-stripe magnetic order, in which FM Cr chains running along y are ordered antiferromagnetically.

Comparing the energies of different states in Fig. 4, we can make several conclusions. First, we see that if the ordering between planes were FM and without extra lattice distortion [Fig. 4(a)], the absolute minimum for the parameters calculated for AgCrS_2 would correspond to the simple 120° AF structure, i.e., state IV in Fig. 4. Such in-plane ordering is indeed realized in LiCrS_2 , but for real AgCrS_2 the observed ordering is different and corresponds to the DS structure.

When we change the interlayer ordering, making it AFM, the situation already changes: the 120° state (state IV) is destabilized, and another state, III, becomes the absolute minimum [Fig. 4(b)]. We also notice that AFM interlayer ordering strongly lowers the energy of the 90° structure [state II in Fig. 4(b)], which, as discussed above, is degenerate with the DS one, so that this state starts to compete with state III. And when we include the lattice distortion present in AgCrS_2 in the LT phase [Fig. 4(c)], DS state II becomes the absolute minimum. Thus, we see that for the lattice corresponding to the real LT structure of AgCrS_2 , DS magnetic ordering with AFM coupling between layers is indeed the ground state in our calculations. We also see that several factors are important for the stabilization of this DS structure: in addition to a particular ratio of different exchange constants (see below), also a particular three-dimensional interlayer ordering and lattice distortion, accompanying magnetic ordering, are important for making the DS structure.

But we also see in Fig. 4 that there exist, especially in the HT lattice, other magnetic states competing with the DS one. Thus, one can predict that the magnetic fluctuations above T_N , which could be probed, e.g., by inelastic neutron scattering, could be most pronounced not at the wave vector corresponding to the DS ground-state structure, but at other values of \mathbf{q} , for instance, those corresponding to solutions III and IV in Fig. 4.

Yet another conclusion which we can extract from Fig. 4 is that, at least in AgCrS_2 , the spin-lattice (magnetostriction) coupling is very important in these systems: only when we included the lattice distortion, occurring in AgCrS_2 below T_N , did we obtain the real DS structure as a ground state.

In addition to the nonrelativistic calculations discussed above, we have also studied the magnetocrystalline anisotropy in MCrS_2 by accounting for spin-orbit coupling in calculations for the FM spin structure with the magnetization directed along different crystallographic axes. It turns out that Cr atoms form an easy-plane magnet, which is consistent with the experimental results:^{9,11,13–15} the spin-orbit coupling rotates all Cr spin magnetic moments into the ab plane even in the HT phase but does not affect the magnetoelastic in-plane coupling or LT lattice distortion.

TABLE II. Different exchange coupling constants (in meV) in the high-temperature phase of $M\text{CrS}_2$ calculated in the LSDA.

M	J_1	J_2	J_3	J_z	J_1/J_3
Li	5.17	0.46	2.73	0.93	1.9
Cu	0.16	0.03	1.51	0.82	0.1
Au	7.41	1.63	5.93	2.93	1.3
Ag	-0.14	-0.13	2.45	0.74	-0.2
Na	-4.06	0.23	2.49	0.09	-1.6
K	-5.45	0.19	2.11	0.05	-2.6

C. Exchange constants

The LSDA exchange parameters estimated for the HT structure of all six $M\text{CrS}_2$ compounds by fitting corresponding $E(\mathbf{q})$ using the Heisenberg model defined by Eqs. (2)–(7) are listed in Table II. We first do not consider the distorted LT phases of AgCrS_2 and AuCrS_2 , because we want to concentrate on general trends observed in this whole class of materials. Detailed results for the LT phases are presented below. The dependence of the exchange constants on U in LSDA + U calculations is discussed in Sec. IV E.

In Table II we see that, with the exception of AuCrS_2 , which deviates from the general trend and is discussed below, the variation of the nearest-neighbor exchange J_1 in the series $M = \text{Li}, \text{Cu}, \text{Ag}, \text{Na}, \text{K}$ clearly correlates with the corresponding structural parameters presented in Table I. With an increase of the size of the M ion and of the Cr-Cr distance, J_1 changes from strongly AFM in LiCrS_2 , with the smallest Li and shortest $d_{\text{Cr-Cr}}$, to strongly FM in KCrS_2 , with the largest K and longest $d_{\text{Cr-Cr}}$, and becomes very small in the Cu and Ag compounds, with intermediate Cr-Cr distances.

We also notice that in all the compounds the third-neighbor exchange J_3 is AFM and rather strong. On the other hand, the second-neighbor exchange J_2 is weak and can, in most cases, be neglected. Apparently it is an interplay of the nearest-neighbor exchange J_1 and the third-neighbor exchange J_3 , which is primarily responsible for the stabilization of one or the other spin structure in the $M\text{CrS}_2$ series.

Taking these considerations into account, it seems reasonable to apply the J_1 - J_3 model to investigate magnetic ordering in $M\text{CrS}_2$. It is well known that the simple J_1 model with AFM $J_1 > 0$ (see, e.g., Ref. 32) gives noncollinear magnetic ground states with $\mathbf{q} = (0, 2/3)$ and angles of 120° between spin magnetic moments. In the J_1 - J_3 model the magnetic energy equals $E_{1,3}(\mathbf{q}) = \epsilon_1(\mathbf{q}) + \epsilon_3(\mathbf{q})$. A simple analysis shows that for positive J_1 and J_3 the wave vector $\mathbf{q}_{\text{IV}} = (0, 2/3)$ is still the global minimum with the energy of $E = -3/2(J_1 + J_3)$. Here we consider only extrema at wave vectors lying on the x and y axes. Other symmetrically equivalent extrema can be obtained by applying $\pm 2\pi/3$ rotations to corresponding \mathbf{q} . The numbering of the minima corresponds to the notations in Fig. 4.

For $|J_1| < 4J_3$ a local minimum appears at $\mathbf{q}_{\text{II}} = (q_x, 0)$ on the x axis, with q_x defined by $\cos(\sqrt{3}\pi q_x) = -J_1/4J_3$. When $J_1 < J_3/2$ another minimum \mathbf{q}_{III} appears also on the y axis, which becomes the global minimum for FM $J_1 < 0$. If $J_1 = 0$, $\mathbf{q}_{\text{III}} = (0, 1/3)$ corresponds to 120° order of third-neighbor spins. As the strength of FM J_1 increases, both \mathbf{q}_{II} and \mathbf{q}_{III} shift

TABLE III. LSDA exchange coupling constants (in meV) for low-temperature phases of AgCrS_2 and AuCrS_2 .

M	J_{1x}	J_{1y}	J_{2x}	J_{2y}	J_{3x}	J_{3y}	J_{zx}	J_{zy}
Au	5.14	2.69	0.70	0.57	3.19	3.24	1.85	1.32
Ag	1.12	-1.36	-0.30	-0.23	2.54	2.62	1.09	0.62

towards zero, until for FM $|J_1| \geq 4J_3$ the two minima merge at $\mathbf{q} = 0$, which becomes the global minimum.

These additional minima at incommensurate \mathbf{q}_{II} and \mathbf{q}_{III} imply the possible formation of helical magnetic order, but the exact picture does depend on the interlayer exchange coupling J_z too,^{9,15} the latter being one possible way to stabilize the magnetic structures observed in the “intermediate” systems $M\text{CrS}_2$ ($M = \text{Cu}, \text{Au}, \text{Ag}, \text{Na}$). In particular, this may be the origin of incommensurate magnetic structures for $M = \text{Cu}, \text{Na}$ or commensurate DSs for $M = \text{Ag}, \text{Au}$.

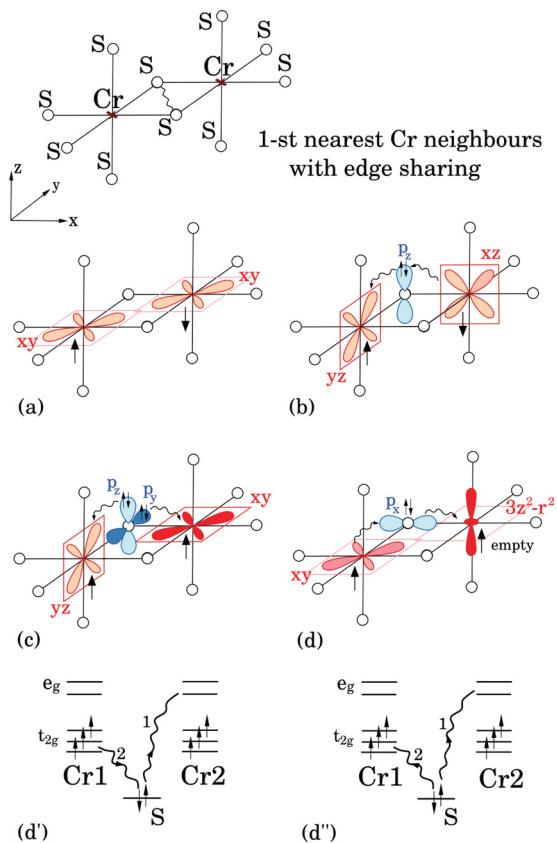
An extra complication is introduced by the observed monoclinic distortion in AgCrS_2 and AuCrS_2 , which induces three pairs of nonequivalent nearest-neighbor exchange couplings: (J_{1x}, J_{1y}) , (J_{2x}, J_{2y}) , and (J_{3x}, J_{3y}) (see Fig. 3). The observed four-sublattice spin arrangement cancels the effect of J_{1x} and J_{2y} . In order to clarify which of the remaining magnetic exchanges are relevant for the stabilization of the DS structure, namely, the FM first-neighbor coupling J_{1y} , the AFM second-neighbor J_{2x} and AFM third-neighbor J_{3x} and J_{3y} superexchanges, and the interplane AFM superexchange J_z , we calculated the energy of different Cr spin moment configurations and derived the corresponding exchange values. The results are summarized in Table III. They show that the monoclinic distortion does stabilize the DS structure by strongly suppressing the AFM contribution to J_{1y} along the FM Cr chains.

We also have to comment on the values of exchange constants for AuCrS_2 listed in Tables II and III. These values definitely deviate from the regularities observed in other materials in this series. The ratio of the important exchange constants J_3 and J_1 for AuCrS_2 is still such that it gives the DS structure observed experimentally. However, the absolute values of these exchanges for this system are about two times larger than what one would expect from a comparison with other materials of this class. We do not have a full explanation for this difference. A possible reason is that AuCrS_2 has a delafossite structure with interlayer Au^+ ions in a linear coordination.¹⁶ It is possible that the reason for the different values of exchange for this system is connected with that. Still, this situation is definitely unsatisfactory, and it requires further study.

D. Interpretation of magnetic properties

Our calculations, presented above, have shown that indeed the observed types of magnetic ordering in the Cr plane in $M\text{CrS}_2$ (120° for Li, DSs for Ag and Au, ferro layers for K) are reproduced. The obtained values of exchange constants (Table II) allow us to explain these magnetic structures.

Thus for the smallest M ion, Li, the nearest-neighbor exchange J_1 is the strongest and AFM; apparently it is predominantly responsible for the observed pure AFM (120°) ordering observed in LiCrS_2 . With increasing Cr-Cr distance


 FIG. 5. (Color online) Different contributions to J_1 .

and Cr-S-Cr angle (Li \rightarrow Cu \rightarrow Au \rightarrow Ag \rightarrow Na \rightarrow K) the value of J_1 decreases and then changes sign, becoming FM for $M =$ Ag, K. Simultaneously the AF exchanges between third neighbors J_3 remains relatively large, and it plays an important role for intermediate compounds Ag/AuCrS₂, apparently leading to their DS ordering. Finally, the large nearest-neighbor ferro interaction J_1 for the large M ion K guarantees ferro ordering in the Cr plane in KCrS₂.

To understand the microscopic origin of different exchange integrals in this series, one should look at different microscope exchange passes. In Figs. 5(a)–5(d) we show the main paths of superexchange, existing in CrS₂ planes with Cr³⁺ ions with d -shell $t_{2g}^3 e_g^0$ and with the geometry of edge-sharing CrS₆ octahedra with a nearest-neighbor Cr-S-Cr angle of about 90°.

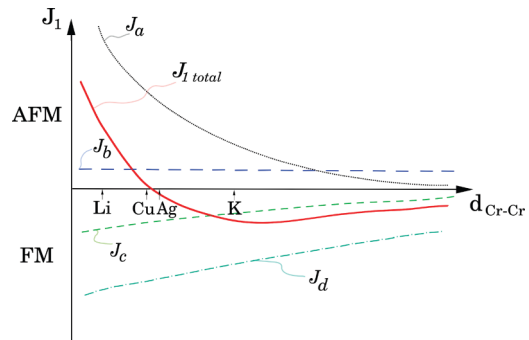
First, there exists a direct overlap of different t_{2g} orbitals of neighboring Cr ions, e.g., the xy orbital in Fig. 5(a). It gives a rather large AF exchange,

$$J_a \sim \frac{t_{dd}^2}{U_{dd}}, \quad (9)$$

which, however, strongly decreases with increasing Cr-Cr distance.

In Figs. 5(b) and 5(c) we show an exchange of t_{2g} - t_{2g} via the 90° Cr-S-Cr bond. The process [Fig. 5(b)] (virtual hopping of t_{2g} electrons through the same ligand p orbital, in this case p_z) gives strong AF exchange,

$$J_b \sim \frac{t_{pd\pi}^4}{\Delta^2} \left(\frac{1}{\Delta} + \frac{1}{U_{dd}} \right), \quad (10)$$


 FIG. 6. (Color online) Schematic dependence of different contributions to the nearest-neighbor Cr-Cr exchange J_1 .

where we denote by Δ the charge-transfer energy [the energy of a transition Cr³⁺(d^3)S²⁻($3p^6$) \rightarrow Cr²⁺(d^4)S⁻($3p^5$)]. One sees that this process does not change strongly with the Cr-S-Cr angle; only the distance Cr-S determines the value of $t_{pd\pi}$ hopping, and this distance is approximately constant in the whole M CrS₂ series.

The process [Fig. 5(c)] (t_{2g} - t_{2g} exchanges via different S p orbitals) leads to an FM exchange, which is, however, usually weaker,

$$J_c \sim -\frac{t_{pd\pi}^4}{\Delta^3} \times \frac{J_{H,S}}{\Delta}, \quad (11)$$

(here $J_{H,S}$ is the Hund's rule coupling on sulfur) and it decreases by absolute value with decreasing Cr-S-Cr angle.

More important is another FM contribution due to the virtual hopping from the occupied t_{2g} shell of one Cr to the empty e_g shells of another Cr [Fig. 5(d)]. As Fig. 5(d) shows, this process also gives the FM contribution,

$$J_d \sim -\frac{t_{pd\sigma}^2 t_{pd\pi}^2}{\Delta^2 U_{dd}} \times \frac{3J_H}{U_{dd}} - \frac{t_{pd\sigma}^2 t_{pd\pi}^2}{\Delta^3} \times \frac{3J_H}{\Delta}, \quad (12)$$

where the first term corresponds to a process [Fig. 5(d')] (effective transfer of an electron from one Cr to the other via S), and the second one corresponds to a process [Fig. 5(d'')] (transfer of two $3p$ electrons of S to the left and right Cr ions). We do not maintain here some numerical coefficients. Note that despite the presence of the small factor $\frac{J_H}{U_{dd}}$ or $\frac{J_H}{\Delta}$, this FM contribution, (12), is comparable with Eq. (9) (typically $t_{pd\sigma} \sim \sqrt{2}t_{pd\pi}$), and also the Hund's rule contribution in Eq. (12) is enhanced by a factor of 3. Thus, though usually the 90° exchange involving a Hund's rule interaction gives FM, but weaker exchange, in this case due to a specific electron occupation of Cr³⁺; it can give a significant contribution and can even start to dominate if the other competitive contributions are small. This is apparently what happens in KCrS₂, in which the main competing AF exchange [Fig. 5(a)] is strongly reduced due to the large size of K⁺ and corresponding increase in Cr-Cr distance. Thus, we can schematically present different contributions to the nearest-neighbor exchange J_1 and their change in the row (Li \rightarrow Cu \rightarrow Au \rightarrow Ag \rightarrow Na \rightarrow K)CrS₂ as follows (Fig. 6).

To explain the resulting magnetic structures, especially the DS structure of AuCrS₂ and AgCrS₂, we also have to include the farther-neighbor exchange. As shown in Table II, the second-neighbor exchange is always small. Somewhat

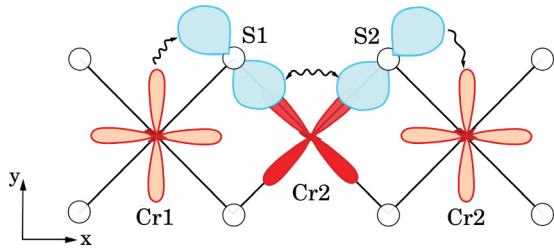


FIG. 7. (Color online) A possible exchange path contributing to the antiferromagnetic exchange of third neighbors J_3 .

surprisingly, larger and more important turns out to be the interaction of third neighbors. This can be schematically explained by the consideration shown in Fig. 7, in which one sees that there is an exchange path connecting occupied t_{2g} orbitals on third neighbors Cr_1 and Cr_3 via two sulfurs, S_1 and S_2 (with their p orbitals being relatively large), due to the p - p overlap or to the overlap via an empty e_g orbital ($x^2 - y^2$) of Cr_2 (Fig. 7).

Thus in this geometry the coupling between third neighbors J_3 turns out to be reasonably large (larger than J_2) and AFM, and in effect, it is this coupling which stabilizes the DS structure for “intermediate” -composition AgCrS_2 and AuCrS_2 , in which the main nearest-neighbor interaction J_1 is small due to the compensation of different contributions to it.

The general tendency showing regular change of different exchange contributions, especially of the nearest-neighbor exchange J_1 (see Fig. 6), is also confirmed by model calculations in which we took LiCrS_2 and artificially compressed it in the c direction, keeping the volume constant. With this change the in-plane Cr-Cr distance and Cr-S-Cr angle increase, following the same trends as in going from LiCrS_2 to (Ag, Au) and to KCrS_2 . Our *ab initio* calculations for this model system confirmed the trend discussed above: with increasing Cr-Cr distance, the large AF coupling J_1 strongly decreases and becomes FM.

The above calculations, carried out in the LSDA framework, are in fact mean-field-like calculations. In principle, in real systems there may also exist quantum effects, i.e., zero-point oscillations. They would be different for different magnetic states, and their contribution in general would somewhat change the energy and relative stability of different phases. However, these effects are usually small for larger spins, and we do not expect them to be significant in our systems, with Cr^{3+} with $S = 3/2$, although the numerical results may change somewhat.

E. The effect of LSDA + U on calculated exchange constants

So far we have discussed only exchange coupling constants determined by fitting $E(\mathbf{q})$ curves calculated within the LSDA (Table II). Comparing the J_1/J_3 ratio in Table II with the critical values obtained from the analysis of the J_1 - J_3 Heisenberg model, one notices that for some of the compounds the estimated J_i do not give an experimentally observed ground state. For KCrS_2 , for example, $J_1/J_3 = -2.6 > -4$ corresponds to an incommensurate spin-spiral structure in the a - b plane instead of experimental FM ordering.

One possible reason for this is that the LSDA underestimates the Coulomb repulsion between rather localized Cr $3d$

electrons. The U_{dd} parameter in expressions (9)–(12) is the energy cost of adding an electron to one of the unoccupied minority-spin t_{2g} state. In LSDA it is governed solely by the exchange splitting of about 2.4 eV between the minority- and the majority-spin t_{2g} states, i.e., by a Hund’s coupling of $3J_H$. As a result, the LSDA overestimates those contributions to intersite exchanges that have U_{dd} in the denominator. Accounting for the Coulomb repulsion in LSDA + U calculations increases the energy difference between the minority- and the majority-spin Cr t_{2g} states by U_{eff} , so that U_{dd} becomes equal to $3J_H + U_{\text{eff}}$.

An increase in U_{eff} suppresses AFM J_a and J_b , whereas the FM t_{2g} - e_g contribution J_d is much less affected. Thus, in compounds with FM J_1 ($M = \text{Na}, \text{K}$) it becomes even stronger, whereas in compounds for which LSDA gives AFM J_1 , its value decreases and it may even change sign. On the other hand, the AFM third-neighbor coupling J_3 , which is governed by the t_{2g} - t_{2g} superexchange (Sec. IV D), gradually decreases with an increase in U_{eff} .

This combined effect of strengthening the FM J_1 and weakening the AFM J_3 leads to a reduction in the J_1/J_3 ratio estimated for KCrS_2 from -2.6 in LSDA to -4.6 and -6.4 in LSDA + U calculations with $U_{\text{eff}} = 1$ and 2 eV, respectively. Thus, accounting for Coulomb repulsion stabilizes the FM in-plane order in KCrS_2 . In LiCrS_2 the 120° structure gives the lowest total energy also in LSDA + U calculations. In other compounds an increase in U_{eff} changes the J_1/J_3 ratio and, consequently, the position of incommensurate minima.

V. SUMMARY

Summarizing, the results of our *ab initio* calculations and the model considerations in Sec. IV D allowed us to explain the very interesting sequence of magnetic phases in layered chromites $M\text{CrS}_2$ with triangular Cr layers, in which the magnetic ordering in Cr layers changes from a purely antiferromagnetic (120°) structure in LiCrO_2 via the “intermediate” double stripe structure of AgCrS_2 and AuCrS_2 (and an incommensurate structure in NaCrS_2 and CuCrS_2) to an ferromagnetic layer in KCrS_2 . These structures emerge mainly as a result of competing contributions to the nearest-neighbor exchange J_1 , together with the reasonably large antiferromagnetic exchange for third neighbors J_3 . In particular, their combined action leads to the most interesting double stripe structure of AuCrS_2 and AgCrS_2 , which apparently is responsible for the multiferroic behavior of the latter (and probably also the former—but this has not been checked yet). Our study demonstrates a quite nontrivial interplay of lattice geometry and orbital occupation giving such diverse magnetic behavior in apparently rather similar materials. The frustrated nature of the lattice definitely plays a very important role in these phenomena. This high sensitivity of magnetic—and apparently some other, e.g., multiferroic—properties to fine details of the electronic and lattice structure could probably be used also to tune the properties of other similar materials. We envisage that further studies of the stability of nuclear and magnetic structures may provide a clue to tailor the magnetoelastic coupling and the multiferroic properties in geometrically frustrated oxides, sulfides, and selenides with different transition metals.

ACKNOWLEDGMENTS

A. V. Ushakov and D. A. Kukusta gratefully acknowledge the hospitality at Max-Planck-Institut für Festkörperforschung in Stuttgart during their stay there. The authors are grateful

to S. Hebert and C. Martin for discussion of experimental situation. The work of A.V.U. and D.I.K. was supported by the European program SOPRANO and by the German projects SFB 608 and FOR 1346.

*Correspondence author: a.yaresko@fkf.mpg.de

- ¹A. P. Ramirez, *Annu. Rev. Mater. Sci.* **24**, 453 (1994).
- ²A. P. Ramirez, C. L. Broholm, R. J. Cava, and G. R. Kowach, *Physica B* **280**, 290 (2000).
- ³A. P. Ramirez, in *Handbook of Magnetic Materials*, Vol. 13, edited by K. H. J. Buschow (Elsevier, North-Holland, Amsterdam, 2001), pp. 423–450.
- ⁴M. F. Collins and O. A. Petrenko, *Can. J. Phys.* **75**, 605 (1997).
- ⁵K. Koumoto, I. Terasaki, and R. Funahashi, *MRS Bull.* **31**, 206 (2006).
- ⁶D. I. Khomskii, *Physics (Trends)* **2**, 20 (2009).
- ⁷S.-W. Cheong and M. Mostovoy, *Nat. Mater.* **6**, 13 (2007).
- ⁸M. Poienar, C. Vecchini, André, A. Paoud-Aladine, I. Margiolaki, A. Maignan, A. Lappas, L. Chapon, M. Hervieu, F. Damay, and C. Martin, *Chem. Mater.* **23**, 85 (2011).
- ⁹F. Damay, C. Martin, V. Hardy, G. Andre, S. Petit, and A. Maignan, *Phys. Rev. B* **83**, 184413 (2011).
- ¹⁰K. Singh, A. Maignan, C. Martin, and Ch. Simon, *Chem. Mater.* **21**, 5007 (2009).
- ¹¹B. van Laar and D. J. W. Ijdo, *J. Solid State Chem.* **3**, 590 (1971).
- ¹²B. van Laar and F. M. R. Engelsman, *J. Solid State Chem.* **6**, 384 (1973).
- ¹³W. Rüdorff and K. Stegemann, *Z. Anorg. Allg. Chem.* **251**, 376 (1943).
- ¹⁴F. M. R. Engelsman, G. A. Wiegers, F. Jellinek, and B. van Laar, *J. Solid State Chem.* **6**, 574 (1973).
- ¹⁵S. J. E. Carlsson, G. Rousse, I. Yamada, H. Kuriki, R. Takahashi, F. Levy-Bertrand, G. Giriat, and A. Gauzzi, *Phys. Rev. B* **84**, 094455 (2011).
- ¹⁶A. Pabst, *Am. Mineral.* **31**, 539 (1946).
- ¹⁷L. K. Alexander, N. Büttgen, R. Nath, A. V. Mahajan, and A. Loidl, *Phys. Rev. B* **76**, 064429 (2007).
- ¹⁸A. Lafond, W. Henggeler, H. Mutka, and B. Ouladdiaf, *Can. J. Phys.* **79**, 11 (2001).
- ¹⁹D. I. Khomskii, *J. Magn. Magn. Mater.* **306**, 1 (2006).
- ²⁰O. K. Andersen, *Phys. Rev. B* **12**, 3060 (1975).
- ²¹A. Perlov, A. Yaresko, and V. Antonov, PY-LMTO, a spin-polarized relativistic linear muffin-tin orbitals package for electronic structure calculations (unpublished).
- ²²J. P. Perdew and Y. Wang, *Phys. Rev. B* **45**, 13244 (1992).
- ²³P. E. Blöchl, O. Jepsen, and O. K. Andersen, *Phys. Rev. B* **49**, 16223 (1994).
- ²⁴L. M. Sandratskii, *J. Phys.: Condens. Matter* **3**, 8565 (1991).
- ²⁵A. N. Yaresko, A. Y. Perlov, R. Hayn, and H. Rosner, *Phys. Rev. B* **65**, 115111 (2002).
- ²⁶A. N. Yaresko, *Phys. Rev. B* **77**, 115106 (2008).
- ²⁷L. R. Mackintosh and O. K. Andersen, in *Electrons at the Fermi Surface*, edited by M. Springford (Cambridge University Press, Cambridge, UK, 1980).
- ²⁸W. E. Pickett, A. J. Freeman, and D. D. Koelling, *Phys. Rev. B* **22**, 2695 (1980).
- ²⁹V. I. Anisimov, F. Aryasetiawan, and A. I. Liechtenstein, *J. Phys.: Condens. Matter* **9**, 767 (1997).
- ³⁰M. T. Czyżyk and G. A. Sawatzky, *Phys. Rev. B* **49**, 14211 (1994).
- ³¹A. N. Yaresko, V. N. Antonov, and P. Fulde, *Phys. Rev. B* **67**, 155103 (2003).
- ³²A. L. Chernyshev and M. E. Zhitomirsky, *Phys. Rev. B* **79**, 144416 (2009), and references therein.